**NUCLEAR
INSTRUMENTS
& METHODS
IN PHYSICS
RESEARCH**
Section A

Measurement of the polarisation of a high energy muon beam

Spin Muon Collaboration (SMC)

B. Adeva [s,19], S. Ahmad [q,15], A. Arvidson [v], B. Badelek [v,x,21], M.K. Ballintijn [n,18], G. Bardin [r],
G. Baum [e,14], P. Berglund [d,g], L. Betev [l,14], I.G. Bird [r,1], R. Birsa [u], P. Björkholm [v],
B.E. Bonner [q,15], N. de Botton [d,r], M. Boutemeur [u,2], F. Bradamante [u], A. Bressan [u],
A. Brüll [e,14], J. Buchanan [q,15], S. Bültmann [a,14], E. Burtin [r], C. Cavata [r], J.P. Chen [w,16],
J. Clement [q,15], M. Clocchiatti [u], M.D. Corcoran [q,15], D. Crabb [w,16], J. Cranshaw [q,15],
T. Çuhadar [d,3], S. Dalla Torre [u], R. van Dantzig [n,18], D. Day [w,16], J.M. Demolis [d],
S. Dhawan [u,15], C. Dulya [b,15], J. Dupont [r], A. Dyring [v], S. Eichblatt [q,15], J.C. Faivre [r],
D. Fasching [p,15,16], F. Feinstein [d,4], C. Fernandez [s,h,19,15,16], B. Frois [r,*], C. Garabatos [s,19,1],
J.A. Garzon [s,h,19,15,16], L. Gatignon [d], T. Gaussiran [q,15], M. Giorgi [u], E. von Goeler [o,16],
A. Gomez [s,h,1,15,16], G. Gracia [s,19], M. Grosse Perdekamp [b,15], D. von Harrach [j,14],
T. Hasegawa [m,17,5], N. Hayashi [m,17], C.A. Heusch [c], N. Horikawa [m,17], V.W. Hughes [y,15],
G. Igo [b,u,14], S. Ishimoto [m,17,6], T. Iwata [m,17], M. de Jong [j,14], E.M. Kabuss [j,14], R. Kaiser [e,14],
A. Karev [i], H.J. Kessler [e,14], T.J. Ketel [n,18], A. Kishi [m,17], Yu. Kisselev [i], L. Klostermann [n,18],
V. Krivokhijine [i], V. Kukhtin [i], J. Kyynäräinen [g], M. Lamanna [u], U. Landgraf [e,14],
K. Lau [h,15,16], T. Layda [c], F. Lehar [r], A. de Lesquen [r], J. Lichtenstadt [t,20], T. Lindqvist [v],
M. Litmaath [n,18], S. Lopez-Ponte [s,h,1,15,16], M. Lowe [q,15], A. Magnon [d,r], G.K. Mallot [d,j,14],
F. Marie [r], A. Martin [u], J. Martino [r], B. Mayes [h,15,16], J.S. McCarthy [w,16],
G. van Middelkoop [n,18], D. Miller [p,15,16], J. Mitchell [w,16], K. Mori [m,17], J. Moromisato [o,16],
G.S. Mutchler [q,15], J. Nassalski [x,21], L. Naumann [d], T.O. Niinikoski [d], J.E.J. Oberski [n,18],
S. Okumi [m,17], D.P. Parks [h,15,16], A. Penzo [u], G. Perez [c,7], F. Perrot-Kunne [r],
D. Peshekhonov [i], R. Piegaia [d,8], L. Pinsky [h,15,16], S. Platchkov [r], M. Plo [s,19], D. Pose [i],
H. Postma [n,18], T. Pussieux [r], J. Pyrlik [h,15,16], J.M. Rieubland [d], A. Rijllart [d], J.B. Roberts [q,15],
M. Rodriguez [s,19], E. Rondio [x,21], L. Ropelewski [x,21], A. Rosado [l,14], I. Sabo [t,20], J. Saborido [s,19],

[1] Now at CERN, 1211 Geneva 23, Switzerland.
[2] Now at University of Montreal, PQ, H3C 3J7, Montreal, Canada.
[3] Permanent address: Bogaziçi University, Bebek, Istanbul, Turkey.
[4] Permanent address: DAPNIA, CEN Saclay, 91191 Gif-sur-Yvette, France.
[5] Permanent address: Miyazaki University, 88921 Miyazaki-Shi, Japan.
[6] Permanent address: KEK, 305 Ibaraki-Ken, Japan.
[7] Permanent address: University of Honduras, Physics Department, Tegucigalpa, Honduras.
[8] Permanent address: University of Buenos Aires, Physics Department, 1428 Buenos Aires, Argentina.
[9] Now at SSC Laboratory, Dallas, 75237 TX, USA.
[10] Now at ESRF, 38043 Grenoble, France.
[11] Now at Philips Kommunikations-Industrie AG, 8500 Nürnberg 10, Germany.

[12] Now at University of Virginia, Dept. of Physics, Charlottesville, 22901 VA, USA.
[13] Now at Warsaw University of Technology.
[14] Supported by Bundesministerium für Forschung und Technologie.
[15] Supported by the Department of Energy.
[16] Supported by the National Science Foundation.
[17] Supported by the Mitsubishi Foundation and Monbusho International Science Research Program.
[18] Supported by the National Science Foundation of the Netherlands (NWO).
[19] Supported by Commision Interministerial de Ciencia y Tecnologia.
[20] Supported by the US–Israel Binational Science Foundation, Jerusalem, Israel.
[21] Supported by KBN.
* Corresponding author.

A. Sandacz [x,21], D. Sanders [h,15,16], I. Savin [i], P. Schiavon [u], K.P. Schüler [y,15,9], R. Segel [p,15,6], R. Seitz [j,14], S. Sergeev [i], F. Sever [18,j], P. Shanahan [16], G. Smirnov [g,i], A. Staude [l,14], A. Steinmetz [j,14], H. Stuhrmann [f,14], W. Tlaczala [x,21,13], K.M. Teichert [l,14], F. Tessarotto [u], W. Thiel [a,11,14], S. Trentalange [b,15], Y. Tzamouranis [r,a,14], M. Velasco [p,15,16], J. Vogt [l,14], R. Voss [d], R. Weinstein [h,15,16], C. Whitten [b,15], R. Windmolders [k], W. Wislicki [x,21], A. Witzmann [e,14], A. Yañez [s,19], A.M. Zanetti [u], K. Zaremba [x,21,13], J. Zhao [f,14]

[a] *University of Bielefeld, Physics Department, 33615 Bielefeld 1, Germany*
[b] *University of California, Department of Physics, Los Angeles, 90024 CA, USA*
[c] *University of California, Institute of Particle Physics, Santa Cruz, 95064 CA, USA*
[d] *CERN, 1211 Geneva 23, Switzerland*
[e] *University of Freiburg, Physics Department, 79104 Freiburg, Germany*
[f] *GKSS, 21494 Geesthacht, Germany*
[g] *Helsinki University of Technology, Low Temperature Laboratory, Otakaari 3A, 02150 Finland*
[h] *University of Houston, Department of Physics, Houston, 77204-5504 TX, and Institute for Beam Particle Dynamics, Houston, 77204-5506 TX, USA*
[i] *JINR, Laboratory of Super High Energy Physics, Dubna, Russian Federation*
[j] *University of Mainz, Institute for Nuclear Physics, 55099 Mainz, Germany*
[k] *University of Mons, Faculty of Science, 7000 Mons, Belgium*
[l] *University of Munich, Physics Department, 80799 Munich, Germany*
[m] *Nagoya University, Department of Physics, Furo-Cho, Chikusa-Ku, 464 Nagoya, Japan*
[n] *NIKHEF, FOM and Free University, 1009 AJ Amsterdam, The Netherlands*
[o] *Northeastern University, Department of Physics, Boston, 02115 MA, USA*
[p] *Northwestern University, Department of Physics, Evanston, 60208 IL, USA*
[q] *Rice University, Bonner Laboratory, Houston, 77251-1892 TX, USA*
[r] *DAPNIA, CE Saclay, 91191 Gif-sur-Yvette, France*
[s] *University of Santiago, Department of Particle Physics, 15706 Santiago de Compostela, Spain*
[t] *Tel Aviv University, School of Physics, 69978 Tel Aviv, Israel*
[u] *INFN Trieste and University of Trieste, Department of Physics, 34127 Trieste, Italy*
[v] *Uppsala University, Department of Radiation Sciences, 75121 Uppsala, Sweden*
[w] *University of Virginia, Department of Physics, Charlottesville, 22901 VA, USA*
[x] *Warsaw University and Soltan Institute for Nuclear Studies, 00681 Warsaw, Poland*
[y] *Yale University, Department of Physics, New Haven, 06511 CT, USA*

A muon beam polarimeter has been built for the SMC experiment at the CERN SPS, for muon energies of 100 to 200 GeV. The beam polarisation is determined from the energy spectrum of positrons from the decay $\mu^+ \rightarrow e^+ \nu_e \bar{\nu}_\mu$. A polarisation of -0.82 is measured with a relative systematic accuracy of 3%.

1. Introduction

High energy muon beams at proton accelerators are produced by pion decay in flight. Due to the parity violating nature of the weak decay $\pi \rightarrow \mu\nu$, such beams are polarised. Experiments using the polarisation of muon beams have measured electroweak effects in the muon–quark interaction [1] and have determined the spin dependent structure functions of the nucleon [2,3]. In the first measurement of the proton spin dependent structure function $g_1(x)$ with a muon beam, the value of the beam polarisation was determined by a Monte Carlo simulation with an estimated accuracy of 7.5% [2]. The SMC experiment is presently being carried out at CERN [4] to measure the spin structure functions of the proton and the deuteron. To reach the goals of the SMC experiment, it is necessary to measure the muon beam polarisation to an accuracy better than 5%. Two methods are used to achieve this goal. The first one determines the beam polarisation from the energy spectrum of positrons from muon decay. A complementary method which has different systematic uncertainties is based on measuring the asymmetry in polarised muon–electron scattering [5]. It will be described in a forthcoming publication. This paper describes the muon decay polarimeter which is now used in the SMC experiment, and the results obtained from experimental runs in 1991 and 1992.

The first measurement of the polarisation of a muon beam was intended to test the prediction of a helicity +1 for the muon from the decay of a negative pion [6]. The experimental technique was to measure the asym-

metry in the production of knock-on electrons from a series of iron foils in which the magnetisation was reversed. The electrons were identified and their energies were measured in a shower detector consisting of plastic scintillators interleaved with the iron foils. The helicity of the muon was shown to be compatible with +1 to an accuracy of 30%.

Because of their interest in measuring parity violation in polarised muon–nucleon deep inelastic scattering, Golovkin et al. [7] measured the polarisation of the muon beam at Serpukov. They used the average value of the positron energy spectrum from muon decay in flight to measure the polarisation difference for oppositely polarised muon beams. The muon beam momentum was measured by a magnetic spectrometer. Downstream of the muon momentum analysing magnet, the beginning of the decay path was defined by a lead filter, designed to absorb incoming electrons. Positrons were identified by calorimetry directly in the beam line. The polarisation difference of 0.8 between the two beams in the momentum range 19–23 GeV was measured to an accuracy of $\simeq 20\%$.

The polarisation of the CERN SPS muon beam was first determined by Bollini et al. [8]. They measured the momentum spectrum of the decay positrons produced along a 300 m decay path. A bending magnet of the muon beam transport system was used to analyse the momentum of the positrons which were identified in a single lead–glass counter. A large error was due to a 10% uncertainty in the muon flux normalisation. The overall error on the polarisation was estimated to range from 10 to 15%. Within this uncertainty, the measured polarisation agreed with a Monte Carlo simulation of the beam phase space and transport system.

2. Experimental method

The longitudinal polarisation of a positive muon emitted in the hadron rest frame at an angle θ^* relative to the momentum of the hadron in the laboratory frame is:

$$P_\mu(\theta^*) = -\frac{E^*\cos\theta^* + p^*}{E^* + p^*\cos\theta^*}, \tag{1}$$

where P_μ is defined in the muon rest frame and all other variables are expressed in the pion rest frame [9]; p^* and E^* are the muon momentum and energy. In terms of kinematic variables measured in the laboratory frame, this formula becomes in the relativistic limit:

$$P_\mu(\theta^*) = -\frac{u - (m_\mu/m_\pi)^2(1-u)}{u + (m_\mu/m_\pi)^2(1-u)}, \tag{2}$$
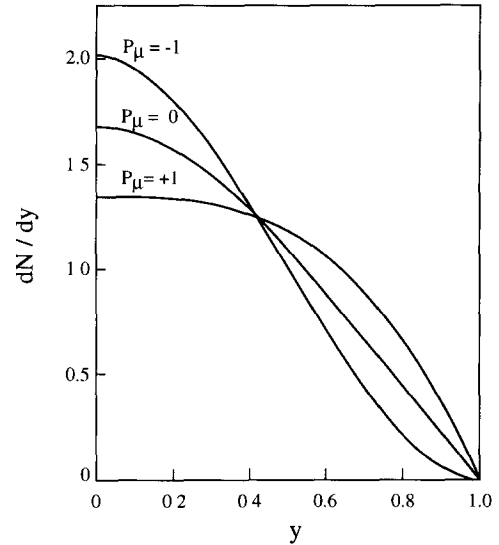

Fig. 1. Energy spectrum of positrons from muon decay, for longitudinal muon polarisations $P_\mu = -1, 0, +1$.

where

$$u = \frac{E_\mu/E_\pi - (m_\mu/m_\pi)^2}{1 - (m_\mu/m_\pi)^2} = \cos^2\left(\frac{\theta^*}{2}\right). \tag{3}$$

The measurement of the energy spectrum of positrons from muon decay in flight, $\mu^+ \rightarrow e^+ \nu_e \bar{\nu}_\mu$, provides a method to measure the muon beam polarisation. In the rest frame of a positive muon, the decay positron is preferentially emitted in the muon spin direction. The positron energy distribution is known as the Michel spectrum [10]. The Lorentz boost produces an energy distribution in the laboratory system which is sensitive to the polarisation of the muon beam. It is given by the expression [11,12]

$$\frac{dN}{dy} = N\left[\frac{5}{3} - 3y^2 + \frac{4}{3}y^3 - P_\mu\left(\frac{1}{3} - 3y^2 + \frac{8}{3}y^3\right)\right]. \tag{4}$$

The variable $y = E_e/E_\mu$ is the ratio of positron and muon energies. At our energies, y is equivalent to the ratio of the momenta of the two particles. N is the number of muon decays. The determination of the spectrum requires the measurement of both the muon and electron momenta.

Fig. 1 shows the positron spectrum for different values of the muon polarisation P_μ. It is particularly sensitive to P_μ at large y, but this region is hard to measure, because the decay positrons are difficult to separate from the high flux region of the muon beam. The central part of the spectrum is more easily accessible with a standard magnetic spectrometer.

Radiative corrections modify the shape of the spectrum given by Eq. (4). These include first order QED
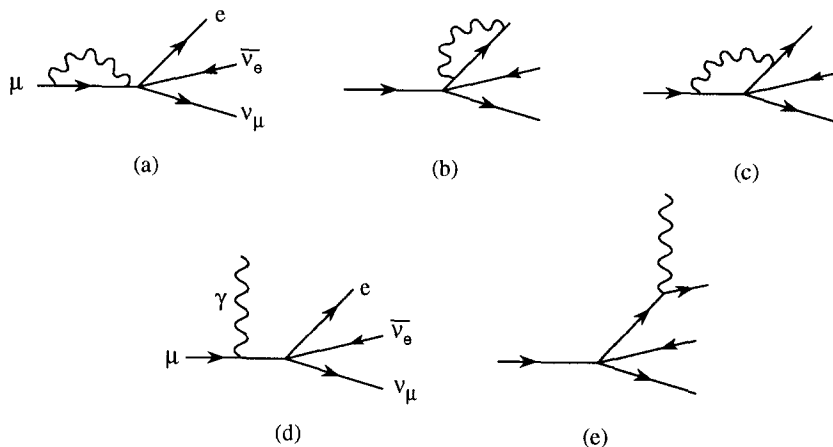
Fig. 2. First order QED diagrams contributing to muon decay. Diagrams (a), (b), and (c) refer to virtual radiative corrections. Diagrams (d) and (e) refer to the radiative decay channel $\mu^+ \to e^+ \nu_e \bar{\nu}_\mu \gamma$.

radiative corrections (Figs. 2a–2c) and contributions from the radiative decay $\mu^+ \to e^+ \nu_e \bar{\nu}_\mu \gamma$ (Figs. 2d and 2e). Fig. 3 shows the decay spectrum of Eq. (4) and the decay spectrum with first order corrections included. The polarisation extracted without these corrections would be different by $\simeq -0.07$

3. The CERN SPS muon beam

The CERN M2 muon beam used for the SMC experiment [13,14] is produced by bombarding a beryllium production target with the 450 GeV SPS proton beam. The secondary hadrons produced are mostly pions, with a kaon admixture that is smaller than 3% for muon beams of 100 GeV energy. Pions and kaons

are momentum selected and transported in a 500 m long decay channel; a fraction of about 10% decays into muons. A 7.7 m long beryllium absorber removes the remaining hadrons. The muon momentum band is defined and the beam halo is eliminated using a system of magnetised iron collimators (scrapers). The maximum muon beam energy is 225 GeV. The SMC experiment operates at a typical intensity of 4×10^7 μ^+/pulse at 100 and 200 GeV. The muon beam pulse has a duration of 2.4 s with a period of 14.4 s. This beam has a circular spot size of about 2 cm FWHM at all critical locations in the experiment.

The polarisation of a muon beam is determined by the momentum bands of both the parent pions and the decay muons accepted by the beam transport system. The measured longitudinal polarisation of the muon beam P_μ is the mean value of $P_\mu(\theta^*)$ over the accepted phase space.

A value of $P_\mu \simeq -1$ is obtained by selecting decay muons emitted at $\theta^* \simeq 0$. A positive value of P_μ is obtained for backward muons. Beams of forward muons have significantly higher intensity than those of backward muons (Fig. 4). Thus, the SMC experiment has chosen to use forward μ^+ beams of 100 and 190 GeV obtained from pion beams of 110 and 210 GeV respectively, both with a polarisation $P_\mu \simeq -0.8$. The polarisation measurements presented in this paper have been obtained with 100 GeV μ^+ from the decay of 110 GeV π^+. A μ^+ beam of 100 GeV from the decay of 165 GeV π^+, with a polarisation $P_\mu \simeq +0.6$, has also been studied.

A Monte Carlo program has been written to model in detail the phase space of parent hadrons and decay muons, and their propagation through the beam transport system [13–15]. The uncertainty in the beam polarisation obtained from this simulation is difficult to
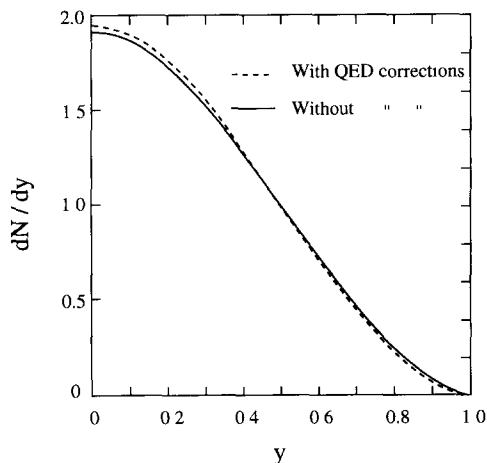

Fig. 3. Effect of first order QED corrections to the decay spectrum calculated for $P_\mu = -0.8$.
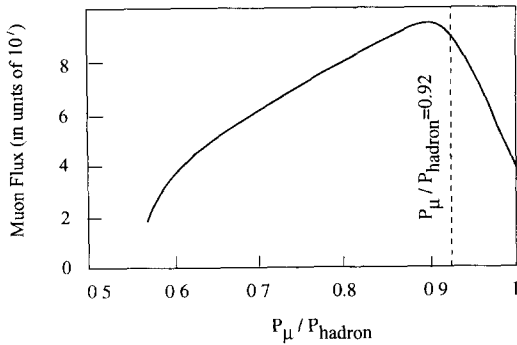
Fig. 4. Maximum muon flux per 10^{12} protons interacting in the target as a function of the ratio p_μ / p_{hadron}.

estimate. This is due largely to a lack of precise knowledge of the secondary pion spectrum, which must be input to the Monte Carlo. Additional uncertainties are due to kaon background in the pion beam, the shape of magnetic fields, the description of all the materials present along the muon beam line, and radiative energy losses of muons in the hadron absorber.

3.1. Muon momentum determination

The beam momentum station (BMS) measures the momentum of incident muons upstream of the SMC experimental hall. It consists of the last set of vertical bending magnets of the beam line and four planes of fast scintillator hodoscopes. Two planes are located upstream of the bending magnets and two planes downstream. Each hodoscope plane consists of 64 scintillators 5 mm wide and 20 mm thick. The resolution of the momentum measurement is 3×10^{-3}.

3.2. Beam phase space

To sample a beam phase space identical to the one seen by the SMC spectrometer, the beam hodoscopes upstream of the SMC polarised target are read out by the polarimeter data acquisition. These hodoscopes consist of 16 planes of scintillation counters. There are 4 planes with counters oriented in the horizontal direction, 4 planes of vertical counters, and 2×4 planes oriented at $\pm 45°$ with respect to the horizontal counters. Each plane consists of 20 elements which are 4 mm wide, 4 mm thick and 9 cm long. The angular resolution is 0.1 mrad and the reconstruction efficiency is higher than 90%.

4. The SMC muon beam polarimeter

Fig. 5 shows the experimental setup. This polarimeter has the following characteristics:
- The parent muon is identified upstream of a field-free decay region.
- The decay positron momentum is measured by a large acceptance magnetic spectometer.
- The decay positron is identified in a lead-glass calorimeter.

The polarimeter is located downstream of the SMC main spectrometer. The last dipole magnet of the beam transport system, located 10 m upstream of the beginning of the decay path, sweeps away most of the positrons which otherwise would contaminate the muon beam. A 33 m long decay path starts at the shower veto hodoscope (SV) and extends to the analysing magnet (MNP26). Along this decay path a telescope of three multiwire proportional chambers (MWPC), labeled PBCs, measures particle tracks before the analysing
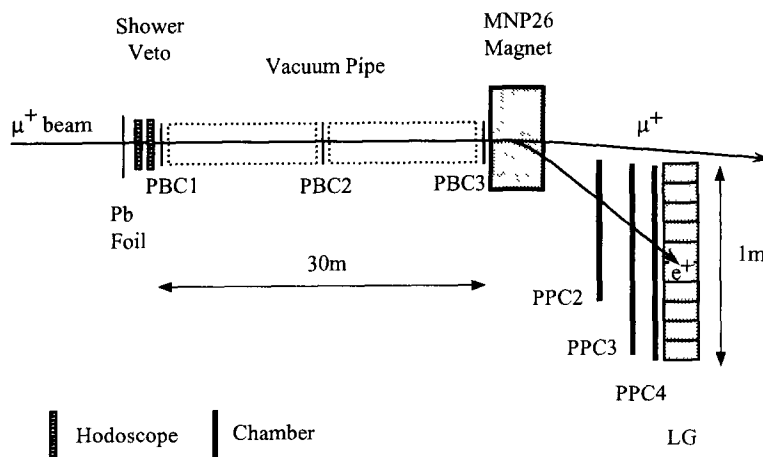

Fig. 5. The SMC muon polarimeter.

magnet. Vacuum pipes are installed along the decay path between the chambers of this telescope to reduce bremsstrahlung of the decay positrons. Downstream of the analysing magnet, a second telescope of three MWPCs, called PPCs, tracks the deflected particles over a distance of 10 m before they reach the lead-glass calorimeter (LG). The positron momentum p_{e^+} is determined from the deflection in the MNP26 magnet as measured by the two MWPC telescopes. The lead-glass calorimeter measures the positron energy E_{e^+}. The positron identification and the background rejection are based on the comparison of the positron energy deposited in the lead-glass calorimeter and the momentum measured by the magnetic spectrometer.

4.1. Muon identification

The shower veto detector (SV) consists of an 8 mm thick lead radiator followed by two hodoscopes, each consisting of 32 plastic scintillation counters with a thickness of 40 mm. Each scintillation counter is equipped with a XP2020 Philips photomultiplier and a base designed to stand high rates. One hodoscope has vertical segmentation while the other one has a horizontal segmentation. In order to limit counting rates to a maximum of 2 MHz in any scintillator, the widths of the hodoscope elements vary from 4 mm in the central region of the beam to 2 cm in the peripheral region. The active surface covered by the shower veto hodoscopes is 20 cm × 20 cm. Positrons produced upstream of the decay path induce showers in the lead radiator and are distinguished from muons in the off-line analysis by their higher pulse heights in the shower veto scintillators.

4.2. Particle tracking

The first wire chamber telescope is located upstream of the MNP26 magnet in the incident muon beam. This telescope consists of three modules of proportional chambers (labeled PBCs) with an active area 20 cm × 20 cm. Each module consists of four planes of wires with 1 mm pitch at four different orientations of 0°, 90°, −45°, 45° with respect to the horizontal plane. The cathodes are made of mylar foils coated with graphite. The chamber thickness is 3×10^{-3} radiation lengths. RMH electronics is used for the readout of the beam chambers. This CERN standard was designed for high counting rates and uses high speed ECL technology [16]. The efficiency of each plane at a rate of 4×10^7 muons/pulse is of the order of 80%. For energies accepted by the spectrometer, decay positrons are emitted with angles less than 2 mrad. No determination is made of the position of the decay vertex.

The second wire chamber telescope is located downstream of the MNP26 magnet. This telescope is formed by three modules of proportional chambers. Each module consists of three planes with 2 mm pitch and wires at three different orientations, with respect to a vertical line, of 0°, 90° and 62° for PPC2, 0°, 60° and −60° for PPC3 and PPC4. The dimensions of these chambers are 50 cm × 50 cm for PPC2 and 120 cm × 35 cm for PPC3 and PPC4. These chambers are equipped with LeCroy PCOSII and PCOSIII readout electronics. The efficiency of each plane is higher than 90%. This telescope accepts decay positrons in the range $0.25 < y < 0.75$. The maximum value of y is determined by positioning the chambers as close as possible to the beam.

4.3. Positron momentum measurement

The analysing magnet MNP26 is a 6 m long, 0.5 m wide H dipole with a gap of 0.14 m. The magnet provides a field of 1.4 T corresponding to a field integral $\int B \cdot dl = 8.5$ Tm. The overall precision on $\int B \cdot dl$ is better than 7×10^{-4}. The accuracy in the measurement of the positron momentum ranges from 0.5% to 1.5%.

The main uncertainty in p_e/p_μ arises from the error in the relative measurement of p_e with the MNP26 spectrometer and p_μ with the BMS. The BMS was calibrated relative to the MNP26 spectrometer by deflecting the muon beam through the polarimeter. The remaining uncertainty arises from surveying errors since the PPC chambers have to be moved into the beam line for the calibration procedure. The resulting systematic error in p_e/p_μ is estimated to be 2×10^{-3}.

4.4. Positron energy measurement

The positron energy is measured in an electromagnetic calorimeter consisting of three rows of 10 blocks each, of SF3 type lead-glass. Each block has a surface of 10×10 cm^2 and is 38.5 cm deep, corresponding to 29.5 radiation lengths; it is viewed by a 3 in. Hamamatsu R2238 fast photomultiplier. The responses of all calorimeter elements were equalised by moving them successively to the same position and measuring their pulse height spectra for the same bin of the e^+ energy spectrum. The energy calibration was done off-line by fitting the ADC channel number to the measured positron momentum. The resolution of the calorimeter is $\sigma_E/E = 0.14/\sqrt{E}$. We have found that an energy threshold of 10 GeV leads to a very efficient discrimination of positrons from muons. This energy is determined by first identifying the signal of maximum amplitude and then summing the signals from adjacent counters with signals larger than 0.5 GeV.

4.5. Trigger

The trigger consists of a fast pre-trigger P1 for chamber strobing (RMH readout) and a final trigger P2 which starts TDCs, gates ADCs, strobes the PCOS readout and provides an event interrupt to the data acquisition. The pre-trigger P1 is an OR of a muon decay pre-trigger and a beam pre-trigger (Fig. 6).

4.5.1. Muon decay pre-trigger

The analog signals from the 30 lead glass blocks are summed. The resulting signal is processed in a double threshold discriminator with a higher threshold corresponding to a minimum energy deposit of 10 GeV. The lower threshold is used as the timing signal since it has smaller walk. The rate of this pre-trigger is 3000/pulse for a beam intensity of 4×10^7 incident muons/pulse.

4.5.2. Beam pre-trigger

Beam particles are identified by a coincidence between the horizontal and vertical shower veto counters. These coincidences are prescaled to sample the beam distribution at a rate of 500 events/pulse. These data are used off-line to study the beam phase space and to provide beam information input for Monte Carlo studies.

The final trigger P2 requires, in addition to both pre-triggers, a single beam particle as measured in the shower veto hodoscopes within 50 ns of the pre-trigger. Multiple beam tracks and electromagnetic backgrounds are rejected by using Majority Logic Units (MaLU). This requirement rejects 60% of the pre-triggers.

5. Data acquisition system

The architecture of the data acquisition is based on the VME processor FIC8232 using the VxWorks UNIX-like real-time operating system. Data from ADCs and TDCs are read via ECL ports and stored into three VME high speed memories. Data from the remaining front end electronics are read via CAMAC interfaces and associated Direct Memory Access modules. The FIC processor is connected to a SUN workstation via a dedicated Ethernet network. This workstation houses the cross-assembler, compiler, linker and all the relevant libraries.

The trigger rate is 1200 events/pulse for a standard beam intensity of 4×10^7 muons/pulse. For each event, 500 bytes are read on average in 600 μs.

All the information from the various detectors is read out in parallel during the beam pulse. The end-of-burst signal triggers the FIC processor to perform the event building which takes about 2 s. The transfer takes about 7 s/pulse and is completed between two beam pulses. The data are stored on 8 mm cassettes using Exabyte tape drives. A detailed on-line monitoring is performed on the SUN workstation. High voltages, pedestals, programmable delays, discriminator thresholds and CAMAC crate status are checked during the time between pulses.

6. Data analysis

The value of the muon beam polarisation is derived from the shape of the positron decay spectrum. This spectrum is determined by reconstructing particle tracks in the polarimeter after applying cuts on the information from the various detectors.

6.1. Event reconstruction

Timing cuts are applied to the BMS to ensure that at least three planes have hits in time with the hits in the shower veto counter. Three BMS planes are the minimum to determine the muon momentum.

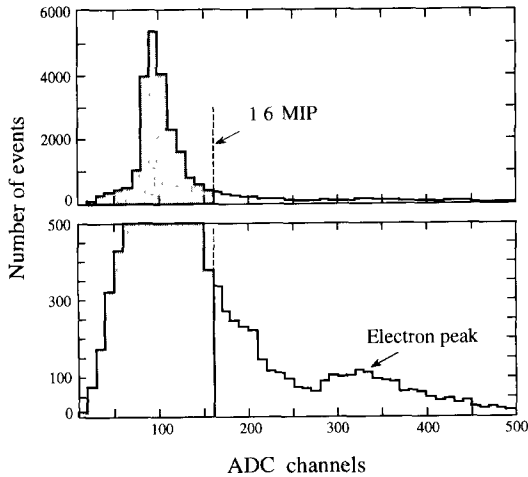Fig. 6. Schematic diagram of trigger logic. The various elements are described in the text.

Fig. 7. Shower veto ADC spectra for muon decay candidates. The large peak is due to the beam muons and the small bump corresponds to background positrons.

Fig. 8. Energy measured by the lead glass calorimeter as a function of tracked momentum.

In the reconstruction of decay events, the muon entering the decay region is correlated with a positron signal in the lead glass calorimeter. This is done by applying timing cuts which require the lead glass and shower veto hits to be in time within ± 3 ns. In addition, the summed pulse height in each shower veto plane has to be smaller than 1.6 times the average pulse height of a minimum ionizing particle (Fig. 7).

We require a single reconstructed track in both the downstream and upstream telescopes. In fitting the upstream track, we take into account that the positron is emitted with an angle smaller than 2 mrad with respect to the muon direction. Three of four planes are required in each PBC beam chamber and two of three planes are required in each downstream PPC chamber. The positron momentum is determined using the magnetic field map of the MNP26 analysing magnet and is compared to the energy of the shower in the lead glass calorimeter (Fig. 8). The band at 45° is due to the positrons from muon decays upstream of MNP26. There is a background due to muons which decay inside the volume of MNP26. Such positrons do not undergo the full deflection expected from the energy measurement and fall to the right of the 45° band. Monte Carlo studies show that a very efficient method of eliminating this background is to require that the upstream and downstream tracks intersect at the center of MNP26. This cut is momentum dependent and has been carefully calibrated. The distributions of simulated decay vertices before and after this cut are shown in Fig. 9. The correlation between the lead glass energy and the reconstructed positron momentum shown in Fig. 8 uses the same cut. The entries in the lower right hand corner correspond to beam muons
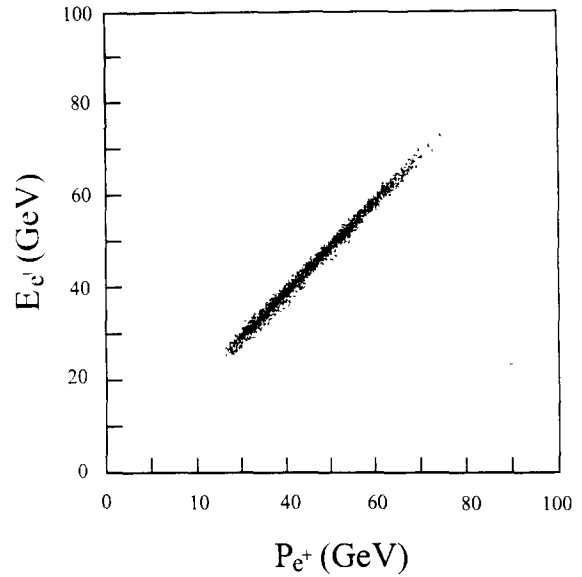
with degraded energy; they are removed by loose cuts on the lead glass energy. The positron fractional energy y is then evaluated from the positron momentum. Fig. 10 shows the y spectrum obtained in 10 h of data-taking.

To determine the background from radiative energy losses in the material upstream of the polarimeter or in the decay region, we have measured the positron spectrum from a negative muon beam. An incident μ^- beam produces a rate of background positrons identi-
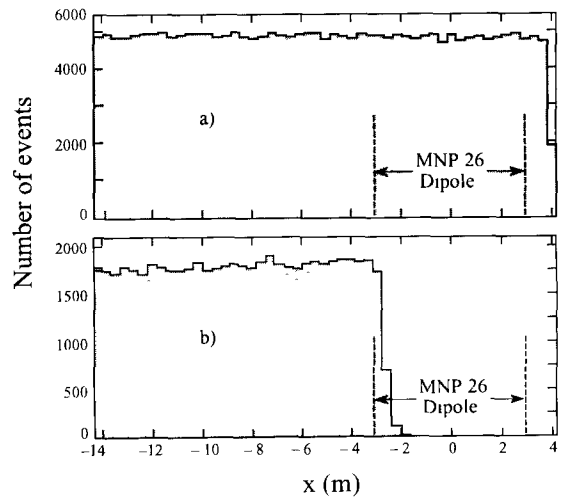

Fig. 9. Monte Carlo generated position of decay vertex. (a) shows the distribution for all generated events. (b) shows the distribution for events passing reconstruction cuts. The position of the analyzing magnet is indicated

cal to that produced by a μ^+ beam. However for our experimental setup, most of the μ^+s which produce background positrons also fall within the polarimeter acceptance. Two charged particle tracks are detected and the event is rejected in the analysis. This is different for negative muons that are bent in opposite direction to e^+. Double tracks corresponding to a correlated $\mu^- - e^+$ pair do not fall within the polarimeter acceptance and are not observed. The positron spectrum created by a μ^- beam is therefore an overestimate of the corresponding background for a μ^+ beam. A Monte Carlo study of this difference shows that for our experimental conditions, the background of positrons from a μ^+ beam is three times smaller than the background measured with a μ^- beam. Taking into account this correction, and the difference in the y dependence between the μ^+ and μ^- background as given by the simulation, leads to a positron backgrounds of 0.8% shown in Fig. 10. Due to the small level of this background and the uncertainty introduced by the Monte Carlo comparison, we have chosen not to subtract the background contribution and instead to include the effect as a component of the systematic error.

6.2. Response function of the apparatus and evaluation of P_μ

The response function A of the spectrometer is computed from a Monte Carlo simulation that also includes first order QED corrections to muon decay [17]. The beam polarisation is then determined using
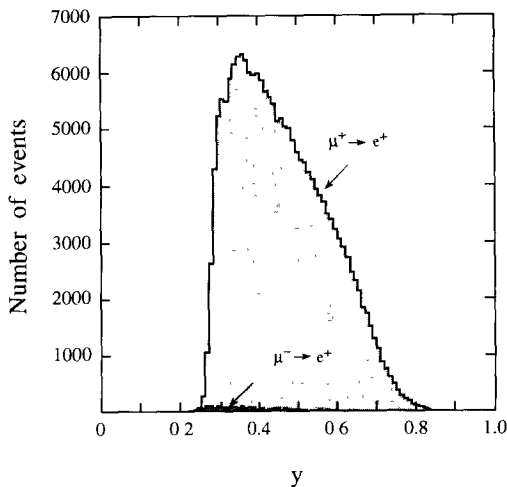

Fig. 10. Measured positron spectrum from 100 GeV μ^+ beam. Also shown is the measured spectrum from $\mu^- \to e^+$. The background rate has been normalized and corrected for the differences in reconstructing events coming from μ^+ and μ^- as discussed in the text.
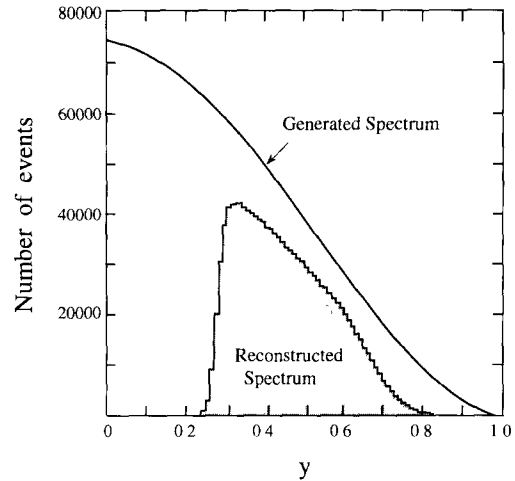

Fig. 11. Monte Carlo simulation of the $\mu^+ \to e^+ \nu \bar{\nu}$ spectrum. The solid curve is the generated decay spectrum Eq. (4) for a polarisation $P_\mu = -0.8$. The Monte Carlo simulation calculates the effect of first order QED corrections at the point of decay and then tracks positrons through the detectors. The shaded histogram represents the events reconstructed by the analysis program.

Eq. (4), after correcting the measured energy spectrum of the positrons for the simulated response function.

To determine the overall response function $A(y)$ of the apparatus, beam muons are generated with position, direction, and momentum obtained from reconstructed experimental beam triggers. All muons are forced to decay between the shower veto and the downstream end of the magnet. Positrons are generated in the muon rest frame according to a decay spectrum for a given polarisation which includes the first order radiative corrections discussed in section 2. As a starting value for the muon polarisation we have taken -0.8, but we have checked that the response function $A(y)$ does not depend on this value when varying P_μ in the range -0.7 to -0.9. The propagation of all particles is simulated using the GEANT program [18] and the measured field map. The measured efficiencies of the downstream chambers, which may distort the observed spectrum, are included in the Monte Carlo simulation; inefficiencies in the upstream chambers have negligible effect on the shape of the measured spectrum and are ignored. The hit information on all chambers and scintillation counters is digitised. The output from this Monte Carlo program is processed by the same analysis program as that used for the experimental data. The reconstructed spectrum is compared to the prediction of Eq. (4) to determine $A(y)$ (Figs. 11 and 12). Correcting for this response function one obtains the decay spectrum shown in Fig. 13.
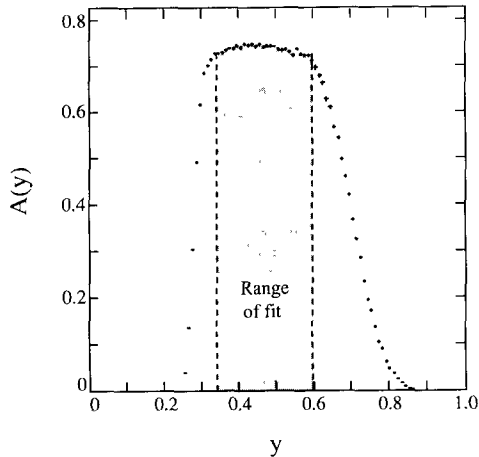
Fig. 12. Response function $A(y)$ as determined from the ratio of the two histograms in Fig. 11. It includes geometrical acceptance, detectors efficiencies and QED corrections. The dashed lines indicate the region of acceptance used for the determination of P_μ from a fit to Eq. (4).

The muon polarisation P_μ is determined by fitting Eq. (4) to the spectrum shown in Fig. 13 allowing P and N to vary freely. The fit is restricted to the region of the response function $A(y)$ $0.34 \leq y \leq 0.6$ for which positrons travel through a region of the spectrometer which is well described by the Monte Carlo simulation (Fig. 12). A polarisation of -0.820 ± 0.035 is obtained from the corrected spectrum shown in Fig. 13. The fall in the response function $A(y)$ on the low-y side of Fig.
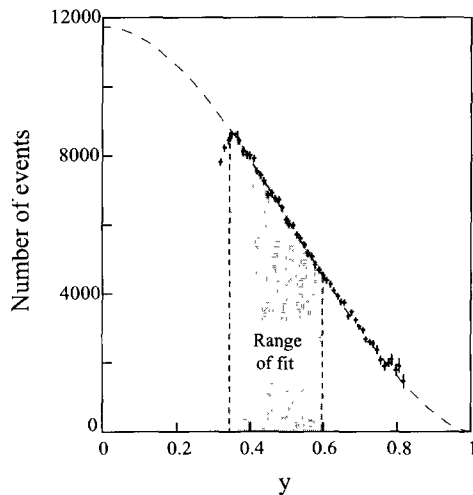

Fig. 13. Corrected decay spectrum. The dashed lines indicate the region of acceptance used for the determination of P_μ from a fit to Eq. (4). The dashed curve is the result of the best fit, which gives a χ^2 of 15.6 for 25 degrees of freedom.

13 is due to the fact that particles in this region fall outside of the downstream proportional chambers.

6.3. Systematic uncertainties

We have evaluated the systematic error on our measurement coming from the uncertainties in p_e/p_μ, positron background, energy loss, radiative corrections and geometrical acceptance by Monte Carlo simulation.

– The uncertainty in the determination of the p_e/p_μ ratio of 2×10^{-3} discussed in section 4.3 leads to a systematic uncertainty in the polarisation of $\sigma(P_\mu)_{p_e/p_\mu} = 0.01$. For the 1991 run, this error turned out to be 0.03 due to a surveying ambiguity.

– The positron background shown in Fig. 10 increases the measured polarisation by $\delta P_\mu = +0.01$. This correction is based on a combination of experimental measurements and a Monte Carlo simulation and has an uncertainty of the same order $\sigma(P_\mu)_{e^+} = 0.011$.

– We assumed a muon beam polarisation of $P_\mu = -0.8$ to calculate radiative corrections in the case of a negatively polarised muon beam and $P_\mu = +0.5$ for a positively polarised beam. In the region of our measurement radiative corrections are essentially independent of the precise value of the beam polarisation. We estimate the contribution to the uncertainty due to radiative corrections to be $\sigma(P_\mu)_{\text{Rad Corr}} = 0.008$.

– Energy losses of the muons and decay positrons can lead to an error in the determination of $y = E_e/E_\mu$. Ignoring this effect would shift the measured polarisation by $\delta P_\mu = -0.05$. We estimate that we can account for these effects to within 10% with our Monte Carlo simulation. Thus, we assume a contribution of $\sigma(P_\mu)_{\text{Energy Loss}} = 0.005$ to the systematic error.

– The contribution to the systematic error due to the Monte Carlo calculated geometrical acceptance which includes detector efficiencies is minimised by restricting the fit to the spectrum to the region of $A(y)$ $0.34 \leq y \leq 0.6$. A systematic error of $\sigma(P_\mu)_{\text{acceptance}} = 0.01$ is estimated for this calculation.

Table 1
Contributions to the total systematic error

Parameter	$\sigma(P_\mu)$
p_e/p_μ	0.011
Radiative corrections	0.008
Energy loss	0.005
Positron background	0.010
Geometrical acceptance	0.010
Total	0.022

Table 2
Experimental results. Calculated values are obtained from the Monte Carlo simulation for the SPS beam as discussed in section 3

| Beam polarization | | | | | |
Year	E_π/E_μ [GeV]	Measured P_μ	Stat. error	Syst. error	Calculated P_μ
1991	110/100	−0.82	0.03	0.03	−0.83 ± 0.05
1992	110/100	−0.84	0.05	0.02	−0.83 ± 0.05
1992	165/100	+0.62	0.06	0.02	+0.53 ± 0.10

The contributions to the systematic error are summarised in Table 1. Adding these contributions in quadrature, we find a total systematic error:

$$\sigma(P_\mu) = 0.022. \tag{5}$$

6.4. Experimental results

We have measured the muon beam polarisation for three different experimental conditions. The results are listed in Table 2. Also listed are the values calculated from a Monte Carlo simulation of the beam line. In order to check the accuracy of our estimate for the total systematic uncertainty we have made an additional measurement of the polarisation for a positively polarised muon beam. As shown in Table 2, Monte Carlo calculations are consistent with all of our measured values.

7. Outlook

This polarimeter measures the polarisation of the CERN SPS 100 GeV μ^+ beam used for the SMC experiment with a statistical accuracy better than 5% in 10 h of data acquisition. We estimate the total systematic uncertainty to be of the order of 3%.

The SMC also collects data with 190 GeV muons. For this case, acceptance limitation and the longer muon decay length necessitate four times longer data taking time to achieve the same statistical accuracy.

This polarimeter will be used to monitor the stability of the muon beam polarisation. In addition, infor-

mation from beam tracking hodoscopes positioned near the SMC polarised target is acquired. This will allow us to study the polarisation of the beam with the same phase space used for the measurement of the spin dependent structure function. The result of these studies will be reported in a later publication.

References

[1] A. Argento et al., BCDMS, Phys. Lett B 120 (1983) 245.
[2] J. Ashman et al., EMC, Phys. Lett. B 206 (1988) 364; Nucl. Phys. B 328 (1989) 1.
[3] B. Adeva et al., SMC, Phys. Lett. B 302 (1993) 533.
[4] The Spin Muon Collaboration (SMC), Measurement of the Spin-Dependent Structure Functions of the Neutron and Proton, CERN/SPSC 88-47 (SPSC/P242) (1988) (unpublished).
[5] P. Schüler, Proc. 8th Int. Symp. on High Energy Spin Physics, Minneapolis, 1988.
[6] G. Backenstoss et al., Phys. Rev. Lett. 6 (1961) 415.
[7] S.V. Golovkin et al., Nucl. Instr. and Meth. 138 (1976) 235.
[8] D. Bollini, P.L. Frabetti, G. Heiman, G. Laurenti, F.-L. Navarria and N. Pinardi, Nuovo Cimento A 63 (1981) 441.
[9] R. Hagedorn, Relativistic Kinematics (Benjamin/Cummings, Reading, Massachusetts, USA, 1963).
[10] T.D. Lee and C.S. Wu, Ann. Rev. Nucl. Sci. 15 (1965).
[11] F. Combley and E. Picasso, Phys. Rep. C 14 (1974) 20.
[12] R. Clifft and J.H. Field, Report EMC 78/29 (unpublished).
[13] R. Clifft and N. Doble, CERN/SPSC/74-12 (CERN/Lab. II/EA/74-2).
[14] N. Doble, L. Gatignon, G. von Holtey and F. Novoskoltsev, this issue, Nucl. Instr. and Meth. A 343 (1994) 351.
[15] Ch. Iselin, HALO, CERN Yellow Report 74-17 (1974).
[16] J.B. Lindsay et al., Nucl. Instr. and Meth. 156 (1978) 379.
[17] F. Scheck, Phys. Rep 44 (1978) 187.
[18] R. Brun et al., GEANT 3 Users Guide, CERN-DD, (1987).